Journal of Colloid and Interface Science 622 (2022) 700–707

Contents lists available at ScienceDirect

Journal of Colloid and Interface Science

journal homepage: www.elsevier.com/locate/jcis

Electro-orientation of Ag nanowires in viscoelastic fluids

Sergio Martín-Martín, Ángel V. Delgado, Paloma Arenas-Guerrero, María L. Jiménez *

Department of Applied Physics, University of Granada, Avda. de Fuente Nueva sn, 18071 Granada, Spain

HIGHLIGHTS

- We study the electro-orientation of nanowires in gelating polymer solution.
- The local complex viscosity governs the orientation randomization of the particles.
- We observe a yield electric field below which particles cannot be oriented.
- This is the minimum field to overcome the mechanical torque exerted by the gel.

GRAPHICAL ABSTRACT

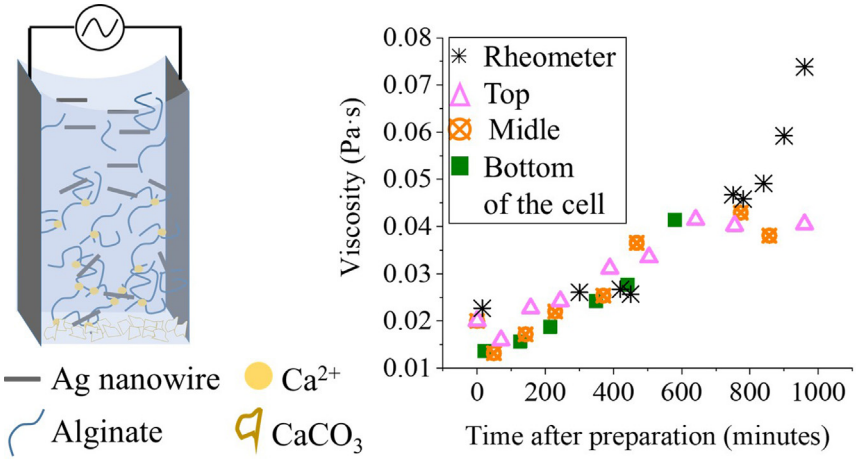

ARTICLE INFO

Article history:
Received 17 February 2022
Revised 18 April 2022
Accepted 27 April 2022
Available online 2 May 2022

Keywords:
Alginate
Silver nanowires
Gel
Electro-orientation
Particle-polymer interactions

ABSTRACT

In this work we study the electro-orientation (through electric birefringence experiments) of silver nanowires in polymer solutions eventually capable of forming gel networks. Information on the structure of the polymer solution is obtained by evaluating the electro-orientation of the nanowires. It is found that in presence of poly(ethylene oxide), Kerr's law (birefringence proportional to the square of the field) is fulfilled, and the randomization process after switching off the external field is purely diffusive, controlled by the viscosity of the Newtonian polymer solution. In the case of (gelating) sodium alginate solutions, measuring at larger distances from the bottom (where the source of cross-linking Ca^{2+} ions is deposited) means a smaller degree of cross-linking, and a less stiff gel. In fact, it is found that after a certain time the birefringence signal gets frozen at the bottom, indicating that a gel network is formed which hinders particle orientation. The viscosity deduced up to that point agrees well with rheological determinations, with increasing deviations found at longer times due to the inhomogeneous gel formation. This process has an interesting consequence on birefringence response: Kerr's law fails to be fulfilled, appearing a "yield" applied electric field, larger the longer the time after preparation.

1. Introduction

The mixtures of hydrogels and nanoparticles in solution are promising systems that combine with advantage the properties of both materials. They can be used for instance in the fabrication of mechanically reinforced materials, biocompatible ferrogels for

* Corresponding author.
E-mail addresses: sergiomartin96@correo.ugr.es (S. Martín-Martín), adelgado@ugr.es (Á.V. Delgado), palomaag@ugr.es (P. Arenas-Guerrero), jimenezo@ugr.es (M.L. Jiménez).

https://doi.org/10.1016/j.jcis.2022.04.164
0021-9797/

tissue engineering, hydrogels for drug delivery or catalytic membranes [1–6].

Since hydrogels are viscoelastic fluids, the shear deformations as those exerted in rheological experiments will provoke both an elastic and viscous response. Furthermore, they can be considered as three-dimensional networks of flexible polymer chains, and the dynamics of the particles immersed in the resulting matrix is coupled to the deformation of the polymer chains. For example, if the gel structure is rigid enough, nanoparticles become trapped and cannot diffuse or react to any moderate external field. This is shown, for instance, in Ref. [2], where they observe that in alginate ferrogels, silica-coated iron particles are partially immobilized, and large magnetic fields must be applied in order for the typical particle chains of magnetorheological fluids to be formed.

Apart from the well known free diffusion in ideal Newtonian fluids or the naive total immobilization in a rigid matrix, micro- and nanoparticles exhibit a plethora of behaviors in between these two cases. In fact, it is usually found that their dynamics deviates from that calculated by using the macroscopic viscoelastic properties, a consequence of the short length scale of diffusion as compared to the large deformation involved in conventional rheology experiments. A vast literature exists about the Brownian diffusion of particles in viscoelastic fluids, which is the basis of microrheological studies. From the initial work of Mason and Weitz [7], several papers are devoted to the study of the viscoelastic properties by examining the Brownian diffusion of microprobes (a technique generally known as microrheology, see e.g. [8–12]). This method has several advantages over classical rheology, since it only needs tiny amounts of material, it is highly non-invasive, explores a broad frequency range, and reveals the viscoelasticity relevant to several phenomena, such as bacteria swimming through a biofilm, drugs penetrating the mucous layer of the lung, flows in microfluidics, polymer reptation, etc. These aspects are revealed in microrheology because Brownian motion involve small-scale fluid deformations that cannot be explored by conventional rheology studies.

Rotation of particles can also be used to explore viscoelastic fluids. The analysis of rotational diffusion as a prove of viscoelasticity has been proposed in Ref. [13] and used, for instance, in [14,15]. In fact, Gutierrez-Sosa et al. [16] found some discrepancies in the elastic moduli obtained from translational and rotational diffusion, since translation involves normal and shear stresses, while rotation only produces a shear on the fluid. The authors conclude that rotational diffusion studies are more suited when the matrix compresibility is unknown. Apart from micron-sized probes, or light scattering techniques, which require high transparency of the sample, an alternative is offered in Refs. [17–20], where the effect of the viscoelastic properties of the medium on the magnetic susceptibility of the mixture fluid-microparticles was investigated.

On one hand, this method has the advantage of avoiding transparency requirements in optical determinations. On the other hand, it requires the use of magnetic particles, this narrowing the applicability. Furthermore, since many subcellular biological structures, such as organelles and viruses, are anisotropic in shape, the use of rotational diffusion to study viscoelasticity in biomaterials should provide a useful counterpart to translational diffusion approaches. For instance, in Ref. [21] it was shown that in mixtures of nanowires and dilute solutions of polymers, the application of low frequency electric fields produces the stretching of the chains, and this, in turn, induces the nanowires alignment, so a small change in the structure of the polymer, undetected by rheological methods, produces a dramatic change in the alignment behavior of the immersed nanowires.

The rotational diffusion of nanoparticles can also reveal local properties, out of the reach of conventional rheological techniques, where a macroscopic deformation of the sample is stressed, and hence, an overall response is observed. A local characterization can reveal, for example, some aspects about gel inhomogeneity, which may determine the performance of a particular application, such as the mechanical properties of elastomers or the control of the mesh size in gel electrophoresis [22,23].

One example is the alginate hydrogel formation. Alginate forms a polymer network under the presence of Ca^{2+}, which attract together two negatively charged alginate chains (monomer valence 1) [24]. Being this a fast process when the source of calcium ions is a highly soluble salt, such as $CaCl_2$, the cross-linking density, hence the viscoelastic properties of the hydrogel, are not homogeneous [25].

The orientational dynamics of nanoparticles immersed in a viscoelastic fluid can be explored in electro-orientation experiments. This is a versatile technique, since any micro- and nanoparticle in the fluid can be oriented by the application of alternating electric fields of a suitable frequency. The dynamics of electro-oriented particles can be followed either by microscope observations, or by electro-optic techniques. For instance, in a typical electric birefringence experiment, the electrically aligned particles produce an optical birefringence that can be determined. This procedure can be used for a broad range of particle sizes, so it has been a standard procedure for the study of nanoparticles and polymers orientation in aqueous solution [26–29]. Rotational diffusion of nanowires can be captured by setting the system in a non-equilibrium aligned configuration induced by an alternating electric field and observing the randomization after switching off the electric field. Interestingly, small displacements from the equilibrium configuration can be detected by measuring the electric birefringence, this making it possible to examine the medium only slightly perturbed.

In this work, we study the dynamics of gelation of alginate by analyzing the *i)* electro-orientation and *ii)* rotational diffusion of silver nanowires (Agnws) immersed in it. The electric birefringence technique is used to characterize both phenomena. We observe that rotational diffusion gradually slows down in response of an increase in the local concentration of Ca^{2+}, being this the imprint of the gelation kinetics. This can be ascertained by measuring birefringence at different positions relative to the Ca^{2+} source. Regarding the electro-orientation of the nanowires, we describe a violation of the Kerr law for low field intensities, with a yield value of the electric field below which particles do not respond to the electric field. In this case, an anomalous transient behavior in the randomization process is observed, as the tendency to a disordered system does not begin immediately after switching off the electric field.

2. Theoretical background

Particles immersed in an aqueous medium polarize under the application of an electric field. In the case of non-spherical particles, the induced dipole is not parallel to the field, and this provokes the appearance of an electric torque that forces the particles to orient their longest axis along the field direction. Due to thermal randomization, the alignment is not perfect, but partial, and it can be quantified by the orientational order parameter of the system, defined as

$$S = \frac{1}{2}\langle 3\cos^2\theta - 1\rangle \tag{1}$$

being θ the angle between the field that produces the orientation and the symmetry axis of the particle, and the angle brackets indicate the average over the sample. This parameter takes a value between $S = 0$ for randomly oriented particles, and $S = 1$ for perfectly aligned systems, respectively. When non-spherical particles are even partially oriented due to the application of the field, the

refractive index n of the sample becomes anisotropic. In this situation, we can define the electric birefringence of the suspension as $\Delta n = n_{\parallel} - n_{\perp}$, where the subscripts refer to the directions parallel and perpendicular to the applied field. The electric birefringence relates to particle orientation as [30]:

$$\Delta n = \Delta n_{sat} S \tag{2}$$

where Δn_{sat} is the saturation birefringence, that is, the value of Δn attained when particles are perfectly aligned. Therefore, we can determine particle electro-orientation by measuring the electric birefringence of the suspension.

2.1. Stationary birefringence

When the electric field is switched on, and after a transient response, the system reaches a stationary orientational order characterized by the parameter S_{DC}, corresponding to a value Δn_{DC} of the electric birefringence. It is well known that the Kerr law is fulfilled for these systems, that is, [31,26]

$$\Delta n_{DC} = KE^2\lambda \tag{3}$$

being E the amplitude of the applied electric field, λ the laser wavelength in the electric birefringence experiment, and K the so-called Kerr constant. This proportionality constant depends on the polarizability of the particles, and this, in turn, on the frequency of the applied field and the properties of the particle and the medium [26,31,28,32]. In the case of Agnws, this system has been extensively studied in Refs. [29,33,35,34,36]. The electric field induces a large dipole on the Ag particle, due to its conductive nature, and this is the only responsible for their orientation at high frequencies. At low frequency, in contrast, cations (anions) close to the negative (positive) pole of the particle accumulate and hinder the dipole, hence decreasing the electric birefringence. This phenomenon occurs for frequencies below around 1 MHz, while for larger frequencies, the electric birefringence spectrum reaches a plateau [36].

On the other hand, polymers in solution can be deformed by the action of an electric field. This result is well known and has been extensively used in the past to calculate some properties of the polymer coils [37–39]. However, it has been demonstrated that for moderate electric fields and high frequency, the polymer is not perturbed [37,39]. Recently, in [21] we observed a synergy between polymer stretching and particles alignment. This effect was observed to disappear at frequencies above 1–10 kHz, where the polymer is not perturbed.

2.2. Transient electric birefringence

When the applied electric field is switched off, the system takes a time to randomize. For a polydisperse system in a purely viscous medium, the system randomizes in a rotational diffusion process, which produces the decay of the electric birefringence in a typically stretched exponential function [40]:

$$\Delta n(t) = \Delta n_0 \exp\left[-(6\Theta t)^{\alpha}\right] \tag{4}$$

where Δn_0 is the electric birefringence when the field is switched off, α is the stretched exponent accounting for the polidispersity of the sample and Θ is the rotational diffusion coefficient, related to the particle geometry and the rheological properties of the medium [29]:

$$\Theta = \frac{3k_B T}{\pi\eta L^3} F_{\Theta} \tag{5}$$

where k_B is the Boltzmann constant, T the absolute temperature, η the medium viscosity, L the length of the particles and F_{Θ} a geometry factor that depends on the shape of the particles.

3. Experimental section

3.1. Materials

All the chemicals were purchased in Sigma Aldrich (USA) except the silver nanowires, that were acquired from PlasmaChem, Germany (PL-AgW50). A TEM characterization of the latter can be found elsewhere [21,29]. The mean length (volume-averaged) of the distribution is 2.0 μm.

The particle nanostructure was studied by energy dispersive X-ray analysis in Ref. [21]. They are composed by a silver core and a thin coating of polyvinylpyrrolidone ($(C_6H_9NO)_n$), which provides a small negative charge, stabilising the particles [41]. In a 1 mM NaCl electrolyte, the zeta potential of the coated particles is -19 ± 3 mV (Malvern Zetasizer NanoZS, Malvern Instruments, UK).

One of the polymers of interest in this work is sodium alginate, which is known to form a network in presence of Ca^{2+} ions. However, it has been observed that using highly soluble salts (such as $CaCl_2$) leads to non-homogeneous cross-linking density, and hence viscoelastic properties [25]. Instead of that, we have chosen a different procedure [2]. In this case, the source of Ca^{2+} ions is $CaCO_3$, which is a poorly soluble calcium salt. As a consequence, the major part of salt is not dissolved, but only dispersed. In this form, Ca^{2+} ions are inaccessible for alginate chains to form the gel. Since the $CaCO_3$ powder consists of grains of 5 micron size or larger, it precipitates in a few seconds (density 2830 kg/m^3). Hence, most part of the source of Ca^{2+} is at the bottom of the cell [42]. Dissociation can be triggered by decreasing the pH. We achieve that with D-glucono-δ-lactone (GDL), which hydrolyses to gluconic acid in presence of water. The acidification of the medium is slow, and so is the release of Ca^{2+} ions. Hence, we proceeded as follows: alginate gels were prepared by first dispersing sodium alginate in distilled water at a concentration of 1 % w/w. The desired amount of $CaCO_3$ to reach 15 mM or 6 mM concentration, and 26.7 mg of GDL were mixed with 5 mL of the sodium alginate solution. Another polymer investigated was poly(ethylene oxide) with molecular weight 4 M (PEO 4 M).

3.2. Methods

The rheological behavior of the polymer solutions investigated was determined with a Haake-Mars III (Thermo Scientific, USA) using concentric cylinders geometry (CC16 Dyn Ti). In order to characterize the linear viscoelastic regime, the sample was subjected to a strain amplitude sweep test at fixed frequency (1 Hz).

The device used for the determination of particle orientation, detailed elsewhere [36], is based on the measurement of the electric birefringence of the samples. Briefly, a He-Ne laser beam traverses a polariser, the Kerr cell, a quarter-wave plate and another polariser, reaching a photodiode. The Kerr cell contains the sample, in which stainless steel electrodes are immersed. When an alternating electric field is applied to the suspension, particle orientation makes the sample anisotropic and, hence, birefringent. This modifies the intensity of the light transmitted by the setup. The electric field intensity was fixed between 10–20 V/mm, in order to always have the same birefringence before switching off the electric field, this ensuring the same degree of initial alignment in the sample.

4. Results and discussion

4.1. Response of Agnws in Newtonian viscous media

Fig. 1 displays the experimental electric birefringence of the Agnws immersed in a 0.25% ww solution of PEO 4 M. We can

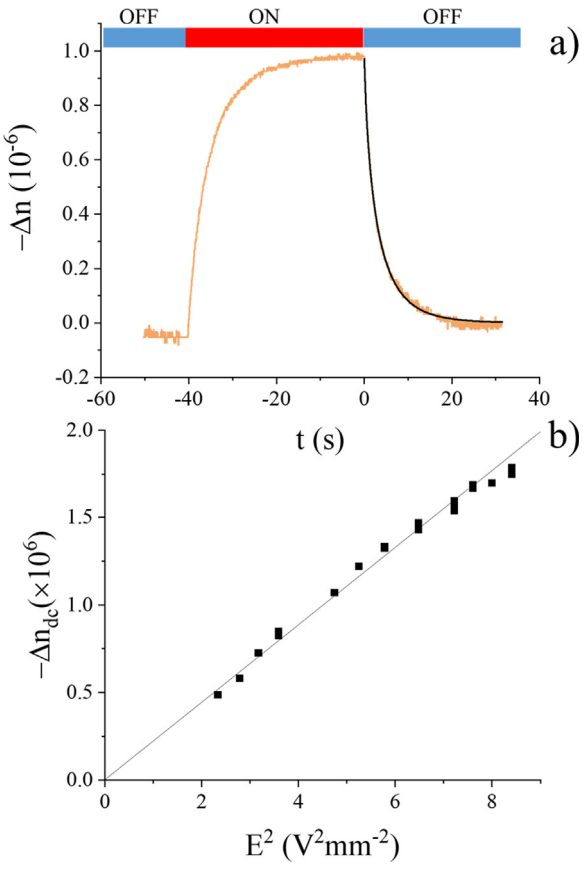

Fig. 1. a) Electric birefringence of Agnws 200 mg/L immersed in a 0.25% PEO-4 M solution as a function of time. $E = 2.7$ V/mm. b) Stationary value of the electric birefringence of the same system as a function of the square of the applied field $\nu = 1$ MHz.

observe that after a transient response, the electric birefringence reaches a stationary value. When the electric field is switched off, the electric birefringence exponentially decays to zero. The origin of this signal can be double, either the polymer or/and the nanowires. On one hand, the polymer may be stretched by the electric field, this producing electric birefringence. This effect has been used in the past to characterize the size of the polymer and its flexibility [37,38,43], but the signal is generally more than two orders of magnitude weaker than that of the nanowires [21]. Furthermore, that signal is not observed for field frequencies above 1 kHz [21,37].

Fitting the transient decay to Eq. 4, we find $\Theta = 0.0481 \pm 0.0007\ s^{-1}$. For elongated particles, the geometry factor can be approximated by:

$$F_\Theta = \log\rho - 0.446 - \frac{0.2}{\log 2\rho} - \frac{16}{(\log 2\rho)^2} \qquad (6)$$

where ρ is the axial ratio, that is L/d, being L the length of the particle and d its diameter.Taking into account the average length and diameter (2.0 μm and 160 nm, respectively [36]), and using Eq. 5, we obtain $\eta = 5.2 \pm 0.1$ mPa·s, close to the value obtained with the rheometer (4.9 mPa·s).

Another relevant characteristic of the birefringence response of nanoparticles immersed in Newtonian fluids is that the Kerr law is fulfilled for moderate field intensities. Several examples are found in literature [26,28,31,32]. In fact, in Fig. 1b we represent the electric birefringence of Agnws immersed in a 0.25% ww PEO 4 M solution as a function of the square of the electric field. Fitting a function $A + BE^2$ to the data, we find a successful linear relation with a negligible y-axis intercept.

4.2. Birefringence response of Agnws in a gelating alginate solution

In Fig. 2a we show the electric birefringence response of Agnws immersed in 1% alginate solution and $CaCO_3$ at different times after adding GDL. We can see that the transient decay becomes slower for longer times.

Next, we fit Eq. 4 to the birefringence decay after switching off the electric field, being τ and α the fitting parameters. In Fig. 2b we show an example. The goodness of this fit (correlation coefficient $R^2 = 0.998$) indicates that the Brownian randomization can be characterized by a rotational diffusion coefficient as that in Eq. 5, from which, we can calculate an "apparent" viscosity. Similar results are found for every examined time, or any position in the Kerr cell, with α around 0.9. A complex rotational diffusion process has been previously described for particles immersed in a gel. In [14] it was found that the rotational diffusion of Au nanoparticles is not free but restricted to 2D, as a consequence of a localized anisotropic compression during the gelation of the medium. Such effect is observed for poly(acrylamide) gel, for which the elastic modulus is three orders of magnitude larger than in the present system.

Since the Ca^{2+} source is located at the bottom, we study three different positions in the sample, corresponding to three heights

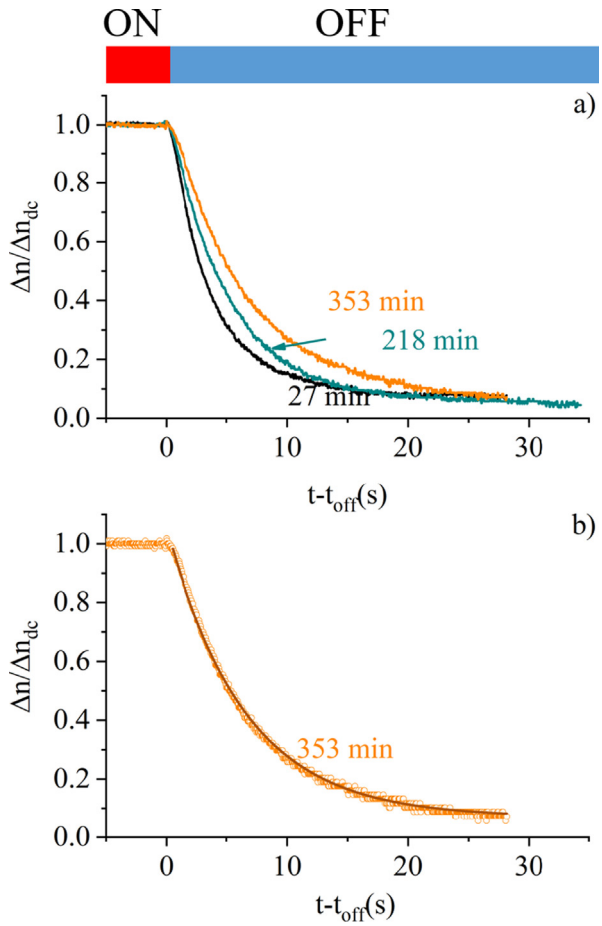

Fig. 2. a) Electric birefringence of 200 mg/L Agnws immersed in alginate solution normalized to the stationary value Δn_{dc}, obtained after the times indicated. In b) pannel the line is the stretched exponential function fitted to the birefringence decay.

in the Kerr cell: A (5 mm), B (9 mm) and C (13 mm). Fig. 3 displays the results for each of these positions. In each case, the last point plotted corresponds to a situation whereby the particles cannot be oriented by the external electric field, indicating a high degree of cross-linking between alginate chains. That is, the gel network imposes a large restriction on their rotation behavior.

However, before reaching this point, there is a significant increase of the viscosity. In Fig. 3 we observe similar results for the three examined positions. Nonetheless, some differences are detected:

- The characteristic gelation time is longer for the upper position.
- That time is one order of magnitude longer when the $CaCO_3$ concentration is lower.
- The viscosity increase is faster than linear in Fig. 3a ($CaCO_3$ 15 mM), while in Fig. 3b ($CaCO_3$ 6 mM) we observe a linear relation followed by a plateau.
- In Fig. 3a, the electro-orientation of the nanowires stops to occur with different viscosity values, indicating a different environment.
- In Fig. 3b we observe the same response at the three locations, indicating that the gel formation is a consequence of uniform dissolution of the salt as the pH becomes more acid.

Additional information can be obtained by analyzing the viscoelastic behavior of the alginate solutions, obtained with the rheometer, as presented in Fig. 4. Note that for small strain of the fluid oscillations, the elastic modulus is similar to the viscous

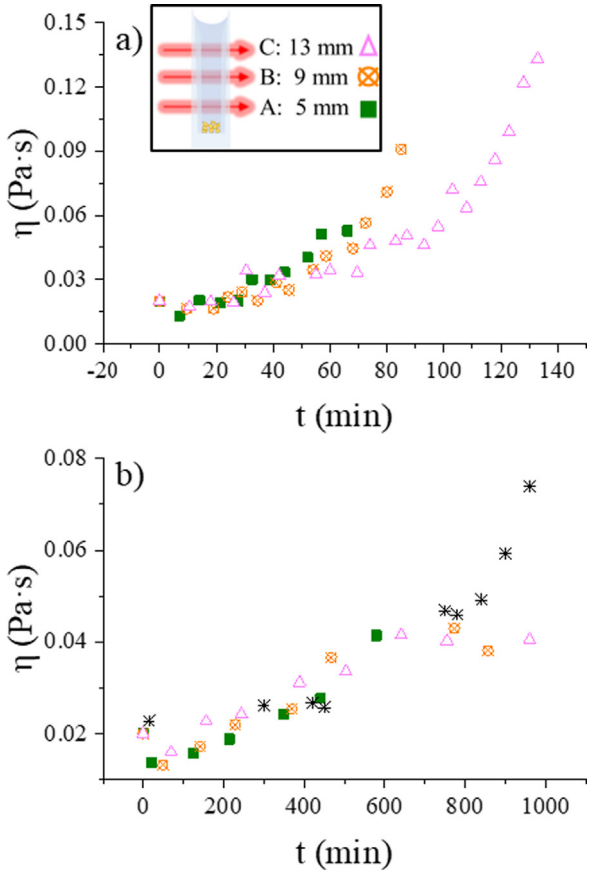

Fig. 3. Viscosity as a function of time of alginate solution in presence of GDL and 15 mM (a) and 6 mM (b) $CaCO_3$, at positions A (full squares), B (open circles) and C (open triangles) in the Kerr cell. Stars are the modulus of the complex viscosity obtained with the rheometer.

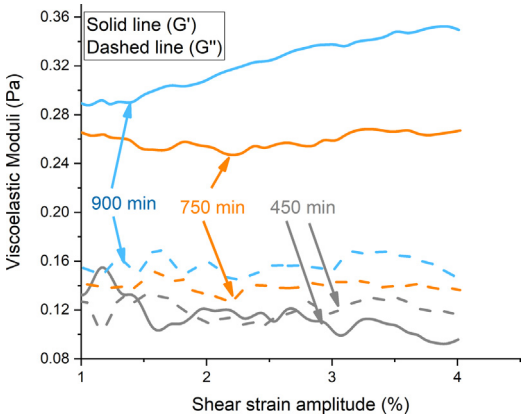

Fig. 4. Elastic ($G\prime$, solid lines) and viscous ($G\prime\prime$, dashed lines) moduli as a function of the strain amplitude for a 1% alginate solution in 6 mM $CaCO_3$ at the times indicated in the plot after adding GDL.

one, shortly after preparing the solution. About 10 h after preparation the elastic modulus starts to increase, while the viscous one does not change appreciably, this indicating that percolation has started. The curing produces a decrease in the mesh size of the hydrogel and an increase of $G\prime$. For the sake of comparison, the modulus of the complex viscosity at 1% strain amplitude is included in Fig. 3b. For short times, we observe a good agreement between these and electric birefringence measurements. Hence, our results show that rotational diffusion kinetics can be well reproduced by the modulus of the complex viscosity, $|\eta^*|$, even in this case in which $|\eta^*|$ is mainly composed by the elastic modulus (Fig. 4), as also reported in [16]. We also observe some deviations for times longer than 600 min after preparation, coinciding with the particles being stuck at the bottom of the cell (Position A in Fig. 3b). Curing takes longer at the top, and hence, the particles can still rotate there. In turn, the overall viscosity as determined by the rheometer is the average of the behavior of the different parts of the sample including the more rigid bottom, and hence, it continues to increase with time (Fig. 3b).

The results in Fig. 3 are the balance between three different processes: *i)* the release of Ca^{2+} ions, *ii)* the growth of crosslinked polymer areas and *iii)* the increase of crosslinking density inside an already crosslinked aggregate. The viscosity variations can be correlated with the increase of crosslinking density in either *(ii)* or *(iii)* mechanisms.

If the increase of crosslinking were only a diffusion-controlled kinetics ruled by a constant Ca^{2+} concentration, we should observe a slowing down of the viscosity increase, but in Fig. 3 we observe the opposite. If it were a growth-controlled mechanism, then the concentration of cations should not have any influence, but in Fig. 3a we observe a faster kinetics than in Fig. 3b. We can conclude that the fact that the rate of viscosity increase is faster with time indicates that process *(i)* plays a significant role.

Since $CaCO_3$ is sparingly soluble, it will initially precipitate in big grains, and only the smaller ones will remain in solution [42]. As a consequence, there is a vertical gradient of Ca^{2+} concentration that produces the non-homogeneous gelation process observed in Fig. 3a. This may also occur in the system of Fig. 3b, but in this case (where a smaller amount of $CaCO_3$ grains is expected), the gradient is too small to be detected by our method. Hence, in Fig. 3b we have similar processes in the upper and lower parts of the cell, while in Fig. 3a we have different scenarios in the same cell.

We can thus imagine the kinetics as follows: before adding the glucono-δ-lactone, the Ca^2 ions have not been released, and no crosslinking can occur. When the pH decreases, Ca^{2+} ions start to be produced by the salt particles (process *(i)*), leading to crosslink-

ing between neighbour polymer chains, which hence form tiny aggregates. Once the ions start to diffuse, these polymer aggregates can grow in size as they find more coils and ions around (process *(ii)*), and eventually become stiffer by increasing the number of crosslinks inside the aggregate (process *(iii)*). Our observation of the gel formation kinetics stops when Agnws become stuck, so they do not align with the external electric field. At this point, the electric torque that tends to align the particles is not intense enough to overcome the polymer resistance to flow. It is not necessary to have a complete percolation throughout the cell, but it is enough to have local percolation events at scales larger than particle size. For this reason, we can have at the same time particle electro-orientation at the upper part of the cell and no movement at the bottom. Hence, it is the growth of the crosslinked polymer aggregates above a certain critical size that makes that Agnws become stuck. Below this critical size, process *(iii)* leads to stiffer aggregates and hence, larger viscosity values, but this process cannot impede the Agnws electro-orientation (particles have to diffuse in a sea of smaller polymer aggregates, but are not trapped inside any of these).

We can use the radius of gyration of alginate coils (about 7 nm), as a rough measure of the average distance which must exist between Ca^{2+} ions in order to have a significant probability of having more than one crosslink between the same coils, that is, to increase the rigidity inside one aggregate (process *(iii)*). This occurs when the ionic concentration in the medium is around 5 mM, and hence it is unlikely in the case of the system of Fig. 3b (average concentration 6 mM), where most of the $CaCO_3$ needs to be dissolved in order to reach such concentration. We can conclude that in the case of Fig. 3a (average concentration 15 mM), the crosslinked aggregates may become stiffer as they increase in size, producing larger viscosities. In contrast, in the case of Fig. 3b, increasing the rigidity of aggregates may occur at the end, when nearly all of the $CaCO_3$ is dissolved. This occurs after reaching the critical size to trap the Agnws, and this can explain that we observe the same maximum viscosity throught the cell.

On the other hand, considering that water is a good solvent for alginate, the correlation length of the polymer (the average distance between neighbour chains) is around 25 nm, and this must be the average distance between Ca^{2+} ions to start crosslinking neighbour alginate coils. This occurs when the ionic concentration in the medium is around 0.1 mM, easily found in both cases. After that, it would be a matter of time to reach the critical size of the percolation in areas for the Agnws to become stuck. During this time, Ca^{2+} concentration continues to grow and the kinetics is accelerated. We can use a model of diffusion-controlled crosslinking process, and taking into account that the concentration of Ca^{2+} C increases with time, we find that the size of the crosslinked aggregate r follows the equation:

$$\frac{dr}{dt} = \xi \frac{C}{r} = \frac{\xi C_0}{r} \frac{t}{t_0} \tag{7}$$

being ξ a proportionality constant and C_0 the concentration at time t_0. This equation is valid while C is increasing and leads to a uniform increase in size with time that can explain the proportionality observed in Fig. 3b until the $CaCO_3$ source starts to run out.

In the case of Fig. 3a the concentration of Ca^{2+} increases faster and reaches larger values, and hence, there is a chance for the aggregates to become more rigid, and this explains that the viscosity increase is accelerated. This picture also applies to the larger viscosity found in the upper part of the cell in Fig. 3a as compared to that in Fig. 3b: during the gel formation crosslinking in the system of Fig. 3a must be faster and lead to larger viscosities.

It is also significant that comparing the bottom of the cell (green squares in Fig. 3a and b), we find similar viscosity values, a further indication that process *(iii)* must occur later, since it is much slower than *(ii)*. In fact in the medium part of the cell, the differences between Fig. 3a and b appear only at the final stages. The balance between these two processes also explains the differences between the bottom and upper parts of the cell in Fig. 3a (green squares and pink triangles). It is observed that in the upper part a larger viscosity is reached before particles become stuck. This is consistent with the fact that process *(ii)* is more likely than *(iii)*.

4.3. Breach of Kerr law

In Fig. 5a we show the electric birefringence of Agnws immersed in alginate solution as a function of the square of the applied electric field, at different times after the sample preparation. At early time, we observe that the Kerr law is roughly fullfiled, as it is usually found[26,36]. In contrast, for longer times we observe that there is a minimum electric field (or yield field, E_y) for the sample to get oriented. At this point, we can represent the data with a modified Kerr law:

$$\Delta n_{dc} = K(E - E_y)^2 \tag{8}$$

where K is a pseudo Kerr constant. Recall that such behavior is not observed when the particles are dispersed in a purely viscous fluid: we found in Fig. 1b that in such a case the only effect of the presence of the polymer in solution is that particle diffusion is slowed down, but Kerr law is satisfied. The existence of a yield field in Fig. 5a suggests that, in order to produce particle rotation, there is a minimum torque that the electric field must exert on the particles

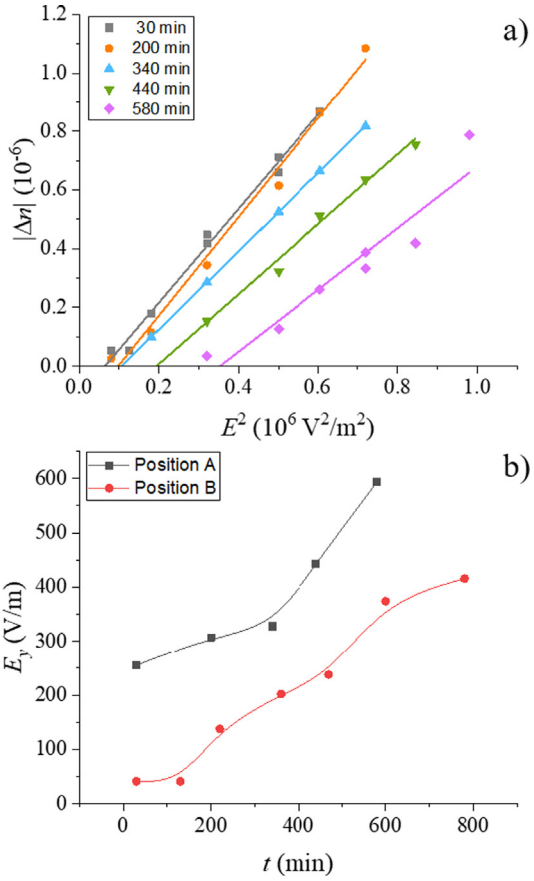

Fig. 5. a) Stationary value of the electric birefringence of a 1% alginate solution in 6 mM $CaCO_3$ as a function of the square of the electric field and for different times after the sample preparation. The lines are the best fit to Eq. 8. b) Yield field of the birefringence in (a) as a function of the time after the sample preparation. Lines are a guide to the eye.

due to the viscoelastic behavior of the fluid. In other words, the existence of a non-negligible elastic modulus produces an initial resistance to flow. Once the yield field is surpassed, the particles can rotate as they would do in a viscous Newtonian fluid (see Fig. 3b). The existence of an initial resistance to flow can also be observed in Fig. 2, where a careful analysis shows that the randomization does not instantaneously follow after switching off the electric field, but lags behind it. In Fig. 5b we represent the yield field as a function of time after sample preparation, and we observe a linear increase, indicating a correlation with the gel formation (as observed in Fig. 3).

5. Conclusions

In this work we have analyzed the electro-orientation of silver nanowires dispersed in polymer solutions. In Newtonian polymers such as poly(ethylene oxide), silver nanowires electro-orientation has a standard behavior, that follows the Kerr's law and with a purely diffusive randomization process, controlled by the particle geometry and the viscosity of the polymer solution. On the other hand, when the the medium has a viscoelastic response, as in the case of alginate hydrogel formation, the transient behavior slows down when the gel starts to be formed and the elastic modulus starts to increase. We have analyzed the kinetics of the sodium alginate gel formation. In this case, the release of the source of cross-linking (Ca^{2+} ions from $CaCO_3$) is controlled by a slow acidification. Contrary to what it was expected [42], we have observed that gel formation in alginate solution does not occur homogeneously throughout the solution, but it is faster close to the Ca^{2+} deposit. Measuring the birefringence at different positions in the Kerr cell allows the evaluation of the viscosity for different stages of the gel formation process. When the mesh size is comparable to the particle length, the latter becomes stuck and can no longer be oriented by the external field. Similar results has been observed in [2], where they found that iron-coated silica particles in alginate solution do not form the typical chains under the action of moderate magnetic fields. The viscosity deduced up to that point agrees well with rheological determinations, with increasing deviations found at longer times. This is explained by the progressive gelation of the solution, producing a significant elastic modulus. This process has an interesting and novel consequence on the birefringence response, as standard Kerr's law fails to be fulfilled, appearing a minimum electric field, below which electro-orientation is not possible. This yield field is a new quantity that may provide some insight about the dynamics of polymers in solution, including gels or entangled polymers, and it can be used to characterize the rheology of solutions with low elastic and/or viscous moduli.

We have presented the first evidence of the local microrheological studies that can be done by the electric birefringence techniques, which may be suited in less accessible media such as the interior of cells or micro- and nano-channels as those used in microfluidics experiments.

CRediT authorship contribution statement

Sergio Martin-Martin: Methodology, Data curation, Validation, Investigation, Formal Analysis. **Ángel V. Delgado:** Writing-Original draft preparation, Funding acquisition, Investigation. **María L. Jiménez:** Conceptualization, Methodology, Investigation, Writing & Editing, Supervision.

Declaration of Competing Interest

The authors declare that they have no known competing financial interests or personal relationships that could have appeared to influence the work reported in this paper.

Acknowledgement

Financial support of this investigation by *Junta de Andalucía*, Spain, European Regional Development Fund (ERDF), and Ministerio de Ciencia, Innovación y Universidades, Spain (Grants No. B-FQM-141-UGR18, P18-FR-3583, A-FQM-492-UGR20 and PGC2018-098770-B-I00) are gratefully acknowledged.

References

[1] E. Senses, S. Narayanan, Y. Mao, A. Faraone, Nanoscale particle motion in attractive polymer nanocomposites, Phys. Rev. Lett. 119 (23) (2017) 237801.
[2] C. Gila-Vílchez, J.D. Durán, F. González-Caballero, A. Zubarev, M.T. López-López, Magnetorheology of alginate ferrogels, Smart Mater. Struct. 28 (2019) 035018.
[3] W. L, L. Zhao, Z. Dai, H. Jin, F. Duan, J. Liu, Z. Zeng, J. Zhao, Z. Zhang, A temperature-activated nanocomposite metamaterial absorber with a wide tunability, Nano Research 11 (7) (2018) 3931–3942.
[4] I. Pastoriza-Santos, C. Kinnear, J. Pérez-Juste, P. Mulvaney, L.M. Liz-Marzán, Plasmonic polymer nanocomposites, Nature Rev. Mater. 3 (10) (2018) 375–391.
[5] M.G. Kim, Y. Shon, W. Miao, J. Lee, Y.K. Oh, Biodegradable graphene oxide and polyaptamer DNA hybrid hydrogels for implantable drug delivery, Carbon 105 (2016) 14–22.
[6] Y. Liu, K. Zhang, W. Li, J. Ma, G.J. Vancso, Metal nanoparticle loading of gel-brush grafted polymer fibers in membranes for catalysis, J. Mater. Chem. A 6 (17) (2018) 7741–7748.
[7] T. Mason, D. Weitz, Optical measurements of frequency-dependent linear viscoelastic moduli of complex fluids, Phys. Rev. Lett. 74 (1995) 1250–1253.
[8] K. Schultz, E. Furst, Microrheology of biomaterial hydrogelators, Soft Matter 8 (2012) 6198–6205.
[9] T.A. Waigh, Advances in the microrheology of complex fluids, Rep. Prog. Phys. 79 (2016) 074601.
[10] B.A. Krajina, C. Tropini, A. Zhu, P. DiGiacomo, J.L. Sonnenburg, S.C. Heilshorn, A. J. Spakowitz, Dynamic light scattering microrheology reveals multiscale viscoelasticity of polymer gels and precious biological materials, ACS Central Sci. 3 (2017) 1294–1303.
[11] A. Espasa-Valdepeñas, J.F. Vega, V. Cruz, J. Ramos, A.J. Müller, J. Martinez-Salazar, Revisiting polymer–particle interaction in peo solutions, Langmuir 37 (13) (2021) 3808–3816.
[12] I. Goychuk, T. Pöschel, Fingerprints of viscoelastic subdiffusion in random environments: Revisiting some experimental data and their interpretations, Phys. Rev. E 104 (2021) 034125.
[13] Z. Cheng, T. Mason, Rotational diffusion microrheology, Phys. Rev. Lett. 90 (2003) 018304.
[14] H. Sun, Z. Wang, Y. He, Direct observation of spatiotemporal heterogeneous gelation by rotational tracking of a single anisotropic nanoprobe, ACS Nano 13 (10) (2019) 11334–11342.
[15] F. Giavazzi, A. Pal, R. Cerbino, Probing roto-translational diffusion of small anisotropic colloidal particles with a bright-field microscope, Eur. Phys. J. E 44 (2021) 61.
[16] C. Gutiérrez-Sosa, A. Merino-González, R. Sánchez, A. Kozina, P. Díaz-Leyva, Microscopic viscoelasticity of polymer solutions and gels observed from translation and rotation of anisotropic colloid probes, Macromolecules 51 (2018) 9203–9212.
[17] E. Roeben, L. Roeder, S. Teusch, M. Effertz, K.D. Ulrich, A.M. Schmidt, Magnetic particle nanorheology, Colloid Polym. Sci. 292 (2014) 2013–2023.
[18] P. Ilg, A.E. Evangelopoulos, Magnetic susceptibility, nanorheology, and magnetoviscosity of magnetic nanoparticles in viscoelastic environments, Phys. Rev. E 97 (2018) 032610.
[19] Y. Raikher, V. Rusakov, R. Perzynski, Brownian motion in a viscoelastic medium modelled by a jeffreys fluid, Soft Matter 9 (2013) 10857.
[20] V.V. Rusakov, Y.L. Raikher, Magnetic response of a viscoelastic ferrodispersion: From a nearly newtonian ferrofluid to a jeffreys ferrogel, J. Chem. Phys. 147 (2017) 124903.
[21] P. Arenas-Guerrero, Á.V. Delgado, S. Ahualli, M.L. Jiménez, Polymer-induced orientation of nanowires under electric fields, J. Colloid Interface Sci. 591 (2021) 58–66.
[22] M. Shibayama, Spatial inhomogeneity and dynamic fluctuations of polymer gels, Macromol. Chem. Phys. 199 (1998) 1–30.
[23] M.Y. Kizilay, O. Okay, Effect of hydrolysis on spatial inhomogeneity in poly (acrylamide) gels of various crosslink densities, Polymer 44 (2003) 5239–5250.
[24] K. Lee, DJ Mooney, Alginate: Properties and biomedical applications, Prog. Polym. Sci. 37 (2012) 106–126.

[25] S. Utech, R. Prodanovic, A. Mao, R. Ostafe, D. Mooney, D. Weitz, Microfluidic generation of monodisperse, structurally homogeneous alginate microgels for cell encapsulation and 3d cell culture, Adv. Healthcare Mater 4 (2015) 1628–1633.
[26] T. Bellini, F. Mantegazza, Electric birefringence spectroscopy: A new electrokinetic technique, in: A. Delgado (Ed.), Interfacial electrokinetics and electrophoresis, Marcel Dekker, New York, 2002, pp. 401–441.
[27] F. Mantegazza, M. Caggioni, M.L. Jiménez, T. Bellini, Anomalous field-induced particle orientation in dilute mixtures of charged rod-like and spherical colloids, Nat. Phys. 1 (2) (2005) 103–106.
[28] M.L. Jiménez, T. Bellini, The electrokinetic behavior of charged non-spherical colloids, Curr. Opin. Colloid Interface Sci. 15 (3) (2010) 131–144.
[29] P. Arenas-Guerrero, Á.V. Delgado, K.J. Donovan, K. Scott, T. Bellini, F. Mantegazza, M.L. Jiménez, Determination of the size distribution of non-spherical nanoparticles by electric birefringence-based methods, Scientific Reports 8 (1) (2018) 1–10.
[30] C.T. O'Konski, Molecular Electro-Optics, Marcel Dekker, 1976.
[31] T. Bellini, F. Mantegazza, V. Degiorgio, R. Avallone, D.A. Saville, Electric polarizability of polyelectrolytes: Maxwell-wagner and electrokinetic relaxation, Phys. Rev. Lett. 82 (1999) 5160–5163.
[32] M.L. Jiménez, L. Fornasari, F. Mantegazza, M.C.D. Mourad, T. Bellini, Electric birefringence of dispersions of platelets, Langmuir 28 (1) (2012) 251–258.
[33] J.J. Arcenegui, P. García-Sánchez, H. Morgan, A. Ramos, Electro-orientation and electrorotation of metal nanowires, Phys. Rev. E 88 (6) (2013) 063018.
[34] J.J. Arcenegui, P. García-Sánchez, H. Morgana, A. Ramos, Electric-field-induced rotation of brownian metal nanowires, Phys. Rev. E 88 (3) (2011) 033025.
[35] J.J. Arcenegui, P. García-Sánchez, H. Morgan, A. Ramos, Electro-orientation of a metal nanowire counterbalanced by thermal torques, Phys. Rev. E 89 (6) (2014) 062306.
[36] P. Arenas-Guerrero, Á.V. Delgado, A. Ramos, M.L. Jiménez, Electro-orientation of silver nanowires in alternating fields, Langmuir 35 (3) (2018) 687–694.
[37] R.S. Wilkinson, G.B. Thurston, The optical birefringence of DNA solutions induced by oscillatory electric and hydrodynamic fields, Biopolym.: Original Res. Biomol. 15 (8) (1976) 1555–1572.
[38] P.J. Hagerman, Investigation of the flexibility of DNA using transient electric birefringence, Biopolym.: Original Res. Biomol. 20 (7) (1934) 1503–1535.
[39] J.M. Kim, T. Ohtani, J.Y. Park, S.M. Chang, H. Muramatsu, DC electric-field-induced DNA stretching for AFM and SNOM studies, Ultramicroscopy 91 (1–4) (2002) 139–149.
[40] T. Bellini, F. Mantegazza, R. Piazza, V. Degiorgio, Stretched-exponential relaxation of electric birefringence in a polydisperse colloidal solution, Europhys. Lett. 10 (1989) 499–503.
[41] A.W. Schell, A. Kuhlicke, G. Kewes, O. Benson, flying plasmons: Fabry-Pèrot resonances in levitated silver nanowires, ACS Photonics 4 (11) (2017) 2719–2725.
[42] W. Tan, S. Takeuchi, Monodisperse alginate hydrogel microbeads for cell encapsulation, Adv. Mater 19 (2007) 2696–2701.
[43] N.C. Stellwagen, Electric birefringence of restriction enzyme fragments of DNA: optical factor and electric polarizability as a function of molecular weight, Biopolym.: Original Res. Biomol. 20 (3) (1981) 399–434.